Int. J. Heat Mass Transfer. Vol. 15, pp. 883–896. Pergamon Press 1972. Printed in Great Britain

TRANSIENT LAMINAR FREE CONVECTION BETWEEN HEATED VERTICAL PLATES INCLUDING ENTRANCE EFFECTS

C. F. KETTLEBOROUGH

College of Engineering, Texas A & M University, College Station, Texas 77843, U.S.A.

(*Received* 27 *November* 1970 *and in revised form* 3 *May* 1971)

Abstract—A numerical study is described of the transient laminar two dimentional motion of a fluid between two heated vertical plates, the motion being generated by a temperature gradient perpendicular to the direction of the body force. Of particular interest is the development of the flow at the entrance region. The results show that, starting from initially still conditions, the velocity builds up at each plate forming two boundary layers which coalesce into one as the fluid moves up between the plates.

For small time the inlet velocity profile at the entrance to the channel has a local minimum on the channel axis and a pair of symmetrically placed maxima on either side of it. However, for small Grashof numbers this entrance profile changes to one with a maximum on the center line for more advanced times. For larger Grashof numbers the entrance profile always has a pair of maxima which develops into a "normal type distribution" as the fluid proceeds up the channel. In all cases both vertical boundaries are at the same constant temperature. Heat transfer characteristics are calculated in terms of the Nusselt number.

Typical temperature and velocity distributions are given for Grashof numbers of 100 and 10000; in both cases the Prandtl number is 0·73. Various numerical techniques are discussed for solving the energy and vorticity equations.

NOMENCLATURE

a, average surface conductance, equation (28);

A, B, a, b, constants in the non-linear transformation, equation (9);

c, specific heat;

d, half separation of the vertical walls;

h_m, average heat transfer coefficient;

H, heat added to fluid;

k, thermal conductivity;

K_x, K_y, defined in equations (18) and (19);

L, height of channel $= w2d$;

m, n, define the entrance size, as shown in Fig. 1, as multiples of the channel width $2d$;

p, pressure;

q, heat flow per unit width of cavity;

t; time;

T, temperature;

T_0, ambient temperature;

T_w, wall temperature;

T_{BC}, temperature along exit boundary BC (see Fig. 1);

u, v, velocity components in x and y directions respectively;

w, ratio of channel height to channel width;

x, y, Cartesian coordinate system defined in Fig. 1;

$\bar{x}, \bar{y}$, linear normalized coordinate system;

$\bar{X}, \bar{Y}$, non-linear coordinate system, equation (9);

Nu_a, Nusselt number, ad/k;

Nu_b, Nusselt number $h_m 2d/k$;

Gr, Grashof number $g\beta (T_w - T_0)(2d)^3/\nu^2$;

Pr, Prandtl number $\mu C/k$;

α, thermal diffusivity;
β, coefficient of cubical expansion;
ρ, density;
μ, dynamic viscosity;
ν, kinematic viscosity;
ψ, stream function;
Γ, vorticity.

All normalized values are indicated by a bar ($\bar{U}$) and are defined in equation (13).

INTRODUCTION

NATURAL convection between two vertical plates has been described by Bodoia and Osterle [1] and Dyer and Fowler [2]. In both cases the flow was assumed to be steady state and the inlet velocity distribution was assumed to be either of a constant magnitude or had a parabolic distribution. Natural convection in a rectangular enclosed cavity has been more extensively investigated (e.g. [3–6]). The form of the equations described in [6] are used here and except for the method of determining the vorticity at the wall, the same procedure has been used.

THEORY

At time $t \leqslant 0$ the vertical plates are assumed to be at ambient temperature T_0 and the fluid is still. For time $t \geqslant 0$ the temperature of the vertical walls at $y = \pm d$ is suddenly raised to a constant temperature T_w. It is assumed that $(T_w - T_0)$ is sufficiently small that the Boussinesq approximation can be made. This neglects density variation in the inertial terms of the equations of motion but retains it in the buoyancy term of the vertical equation. It is also assumed that all over relevant thermodynamic and transport properties are independent of temperature and that compressibility and dissipation effects can be neglected.

The basic equations of transient laminar free convection are the Navier–Stokes equations

$$\frac{\partial u}{\partial t} + u\frac{\partial u}{\partial x} + v\frac{\partial u}{\partial y} = -\frac{1}{\rho}\frac{\partial p}{\partial x} + g\beta(T - T_0) + \nu\left\{\frac{\partial^2 u}{\partial x^2} + \frac{\partial^2 u}{\partial y^2}\right\} \quad (1)$$

$$\frac{\partial v}{\partial t} + u\frac{\partial v}{\partial x} + v\frac{\partial v}{\partial y} = -\frac{1}{\rho}\frac{\partial p}{\partial y} + \nu\left\{\frac{\partial^2 v}{\partial x^2} + \frac{\partial^2 v}{\partial y^2}\right\} \quad (2)$$

the continuity equation

$$\frac{\partial u}{\partial x} + \frac{\partial v}{\partial y} = 0 \quad (3)$$

and the energy equation

$$\frac{\partial T}{\partial t} + u\frac{\partial T}{\partial x} + v\frac{\partial T}{\partial y} = \alpha\left\{\frac{\partial^2 T}{\partial x^2} + \frac{\partial^2 T}{\partial y^2}\right\}. \quad (4)$$

The vorticity equation is derived by combining equations (1) and (2) to remove the pressure term and simplifying by using equation (3) to obtain

$$\frac{\partial \Gamma}{\partial t} + u\frac{\partial \Gamma}{\partial x} + v\frac{\partial \Gamma}{\partial y} = -g\beta\frac{\partial T}{\partial y} + \nu\nabla^2\Gamma \quad (5)$$

the stream function equation

$$\Gamma = \frac{\partial v}{\partial x} - \frac{\partial u}{\partial y} = -\nabla^2\psi \quad (6)$$

the velocity equation

$$u = \frac{\partial \psi}{\partial y}, \qquad v = -\frac{\partial \psi}{\partial x}. \quad (7)$$

The continuity equation is automatically satisfied by equation (7).

These equations are solved for the flow through a vertical channel as shown in Fig. 1 and, because information is lacking about the velocity and vorticity at the entrance AD, for the inflow region as well. At some distance from the entrance, assumptions are made about the velocity distribution. At a distance in the horizontal direction equal to $\pm m$ times the gap between the vertical plates the u and v velocity components were made equal to zero. At a distance downwards in the vertical direction equal to n times the plate height the

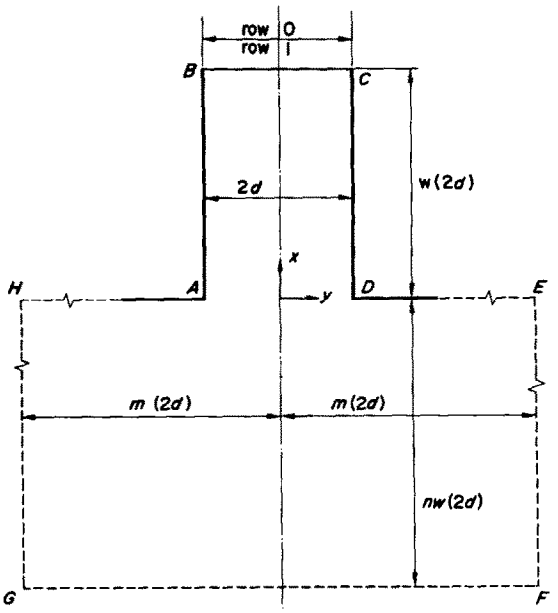

FIG. 1. Physical system showing coordinate system and dimensional details.

velocity distribution was assumed to be fully developed such that $\partial u/\partial x$ was equal to zero at the line GF. This also states that $v = 0$ here. Although St. Venant's principle is often invoked in solid mechanics the same principle can be used in fluid mechanics. If these artificial boundaries are sufficiently far away, the velocity distribution at the entrance AD is not affected, hence, the configuration is essentially a stepped channel. It was necessary to carry out numerical experiments to ascertain that these artificial barriers are sufficiently far away from the entrance to have very little effect.

NORMALIZATION

The spatial normalization is carried out in two stages. Firstly, a linear transformation given by

$$x = 2wnd\bar{x}; \qquad y = 2md\bar{y}$$

and thus when

$$\begin{aligned} &x = 0, \bar{x} = 0; && y = 0, \bar{y} = 0 \\ &x = 2wd, \bar{x} = 1/n; && y = \pm d, \bar{y} = \pm \frac{1}{2m} \\ &x = -2wnd, \bar{x} = -1; && y = \pm 2md, \bar{y} = \pm 1. \end{aligned} \tag{8}$$

The second transformation squeezes the coordinates so that the grid lines in the physical system are closer together at the origin of coordinates. The equations are

$$\begin{aligned} \bar{x} &= A\bar{X}^a + (1 - A)\bar{X} \\ \bar{y} &= B\bar{Y}^b + (1 - B)\bar{Y}. \end{aligned} \tag{9}$$

The indices a and b cause the squeeze effect whilst the second term involving the constants A and B are introduced to avoid a singularity in the derivatives at the origin. From

$$\frac{\partial}{\partial \bar{x}} = \frac{1}{Aa\bar{X}^{a-1} + (1 - A)} \cdot \frac{\partial}{\partial \bar{X}} \tag{10}$$

it can be seen that when $\bar{X} = 0$ a singularity would occur if $A = 1$. Moreover, a non-zero value for A can be chosen so that the boundaries of the vertical channel are at a suitable distance from the origin. After some numerical experiments the following values were selected. The indices a and b were chosen to be 5. The constants A and B were calculated so that

$$\begin{aligned} \bar{Y} &= \pm \tfrac{1}{4} \quad \text{when} \quad \bar{y} = \pm \frac{1}{2m} \\ \bar{X} &= + \tfrac{1}{2} \quad \text{when} \quad \bar{x} = + 1/n. \end{aligned} \tag{11}$$

When m and n are both equal to 30 the values of A and B, using equations (9), are 0·9956 and 0·937, respectively. The other limits of the $\bar{X}$ and $\bar{Y}$ values are

$$\begin{aligned} &\bar{x} = 0, \bar{X} = 0; && \bar{x} = -1, \bar{X} = -1 \\ &\bar{y} = 0, \bar{Y} = 0; && \bar{y} = \pm 1, \bar{Y} = \pm 1. \end{aligned} \tag{12}$$

It is noted that for $\bar{X}$ and $\bar{Y}$ to have the correct signed values the indices a and b must be odd.

With the values of a, b, m and n as selected above, the distance to the artificial boundaries are as shown in Fig. 2. These distances are also given as multiples of d, half the channel width. Some typical values showing the relation be-

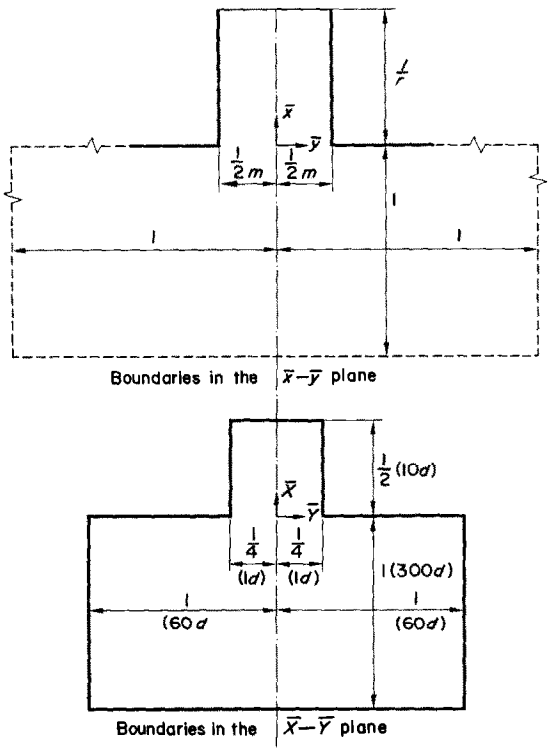

FIG. 2. Normalized coordinate systems.

tween the values of the non-linear variables $\bar{X}$ and $\bar{Y}$ and the physical dimensions, given as multiples of d, are shown in Table 1.

The equations are expressed in the $\bar{X}$–$\bar{Y}$ coordinate system and programmed using finite-difference techniques using constant values of $\Delta\bar{X}$ and $\Delta\bar{Y}$ (not necessarily the same). Table 1 clearly illustrates that, at the origin, a finer mesh in the physical plane is used. At increasing distances from the origin the physical mesh becomes much coarser where velocity changes are much smaller.

The equations are normalized as follows

$$\begin{aligned} Gr &= g\beta(T_w - T_0)(2d)^3/\nu^2 \\ Pr &= \mu C_p/k \\ T &= (T_w - T_0)\bar{T} + T_0 \\ u &= \frac{\nu}{2d}\bar{U} \\ v &= \frac{\nu}{2d}\bar{V} \\ t &= \frac{(2d)^2}{\nu}\bar{t} \\ \psi &= \bar{\psi}\nu \\ \Gamma &= \bar{\Gamma}(\nu/4d^2). \end{aligned} \tag{13}$$

The equations in dimensionless form are

$$\frac{\partial\bar{\Gamma}}{\partial\bar{t}} + \frac{\bar{U}}{K_x}\frac{\partial\bar{\Gamma}}{\partial\bar{X}} + \frac{\bar{V}}{K_y}\frac{\partial\bar{\Gamma}}{\partial\bar{y}} = \frac{Gr}{K_y}\cdot\frac{\partial\bar{T}}{\partial\bar{Y}} + \bar{\nabla}^2\bar{\Gamma} \tag{14}$$

$$\frac{\partial\bar{T}}{\partial\bar{t}} + \frac{\bar{U}}{K_x}\frac{\partial\bar{T}}{\partial\bar{X}} + \frac{\bar{V}}{K_y}\frac{\partial\bar{T}}{\partial\bar{Y}} = \frac{1}{Pr}\bar{\nabla}^2\bar{T} \tag{15}$$

$$\bar{\nabla}^2\bar{\psi} = -\bar{\Gamma} \tag{16}$$

$$\bar{U} = \frac{1}{K_y}\cdot\frac{\partial\bar{\psi}}{\partial\bar{y}}; \qquad \bar{V} = -\frac{1}{K_x}\cdot\frac{\partial\bar{\psi}}{\partial\bar{X}} \tag{17}$$

where

$$K_x = wn[Aa\bar{X}^{a-1} + (1 - A)] \tag{18}$$

$$K_y = m[Bb\bar{Y}^{b-1} + (1 - B)] \tag{19}$$

$$\bar{\nabla}^2 = \frac{1}{K_x^2}\left[\frac{\partial^2}{\partial\bar{X}^2} - \frac{wnAa(a-1)\bar{X}^{a-2}}{K_x}\cdot\frac{\partial}{\partial\bar{X}}\right] + \frac{1}{K_y^2}\left[\frac{\partial^2}{\partial\bar{Y}^2} - \frac{mBb(b-1)\bar{Y}^{b-2}}{K_y}\cdot\frac{\partial}{\partial\bar{Y}}\right]. \tag{20}$$

Table 1. *Relation between normalized values* $\bar{X}$ *and* $\bar{Y}$ *and the ratios* x/d *and* y/d *for chosen values of* a = 5, b = 5, m = 30 *and* n = 30

$\pm\bar{Y} = 0$	0·05	0·10	0·15	0·20	0·25	0·30	0·40	0·50	0·75	1·0
$\pm\frac{y}{d} = 0$	0·189	0·379	0·571	0·774	1·0	1·271	2·088	3·647	16·18	60·0
$\bar{X} = 0·5$	0·4	0·3	0·2	0·1	0	−0·1	−0·3	−0·5	−0·7	−0·9	−1·0
$\frac{x}{d} = 10·0$	3·59	1	0·360	0·135	0	−0·35	−3·60	−10·0	−51·0	−177·6	−300·0

The boundary conditions are

$$\bar{t} \leqslant 0;\ \bar{U} = 0;\ \bar{V} = 0;\ \bar{T} = 0$$

for

$$-1 \leqslant \bar{X} \leqslant \tfrac{1}{2},\ -1 \leqslant \bar{Y} \leqslant 1$$

$$\bar{t} > 0 \begin{cases} \bar{T} = 1,\ \bar{U} = 0,\ \bar{V} = 0 \\ \quad \text{for } 0 \leqslant \bar{X} \leqslant \tfrac{1}{2},\ \bar{Y} = \pm \tfrac{1}{4} \\ \partial\bar{T}/\partial\bar{X} = 0,\ \partial\bar{T}/\partial\bar{X} = 0,\ \partial\bar{U}/\partial\bar{X} = 0, \\ \quad \bar{V} = 0, \text{ for } \bar{X} > \tfrac{1}{2},\ |\bar{Y}| \leqslant \tfrac{1}{4} \\ \bar{T} = 0,\ \partial\bar{U}/\partial\bar{X} = 0,\ \bar{V} = 0, \\ \quad \partial\bar{T}/\partial\bar{X} = 0 \text{ for } \bar{X} = -1,\ |\bar{Y}| \leqslant 1 \\ \bar{T} = 0,\ \bar{U} = 0,\ \bar{V} = 0, \\ \quad \text{for } \bar{X} = 0,\ \tfrac{1}{4} \leqslant |\bar{Y}| \leqslant 1 \\ \bar{T} = 0, \text{ for } -1 \leqslant \bar{X} \leqslant 0,\ -1 \leqslant \bar{Y} \leqslant 1. \end{cases} \quad (21)$$

However, due to symmetry along the center line, it is only necessary to apply the equations to one half of the field using the following boundary conditions at $\bar{Y} = 0$

$$\bar{t} > 0, \frac{\partial\bar{T}}{\partial\bar{Y}} = 0, \frac{\partial\bar{U}}{\partial\bar{Y}} = 0, \bar{V} = 0, \bar{\Gamma} = 0. \quad (22)$$

At the upper boundary BC it was assumed that the fluid as it rises beyond the channel remains approximately the same width for one mesh length, i.e. does not start to spread out. Also, as there is no heat addition beyond BC, the boundary condition is assumed to be

$$\bar{U}, \bar{\Gamma}, \bar{T} \text{ at row '0'} = \bar{U}, \bar{\Gamma}, \bar{T} \text{ at row '1'}$$

(see Fig. 1).

This is the same as saying that the derivatives of these functions are zero at exit and the boundary condition becomes that of fully developed flow. This assumption is restrictive and could influence the flow pattern in the channel. However, in the absence of other information this is the best assumption available.

Row '0' does not actually exist; these boundary conditions are incorporated into the finite difference equation for row 1.

NUMERICAL CONSIDERATIONS

There are several methods for solving the governing vorticity and energy equations. There are:

(a) The Alternating Direction Implicit (ADIP) method as used by Wilkes and Churchill [6]

(b) The Alternating Direction Explicit (ADEP) method described in [7–10].

(c) The Simple Explicit (SE) method as used by MacGregor and Emery [11] which uses a forward difference formula for the time derivative.

(d) The Central Difference Explicit (CDE) method used by Fromm [12] using a central difference formula for the time derivative.

All these methods were tried. The ADIP method suffers from the serious disadvantage that the boundary values of the vorticity are these calculated from the previous velocity fields and hence the boundary values are always one time interval behind the rest of the values. Initially the vorticity is zero around the boundaries and if the discretion is sufficiently accurate the vorticity at the boundary should always remain zero. In [6] vorticity is updated at the boundary by using higher order formula for the velocity derivatives where appropriate. Moreover, it was found that when numerical studies were carried out on a two dimensional model of the equations (i.e. $\partial/\partial x = 0$) the temperature field converged to $\bar{T} = 1$ but the u velocity field continued to update for many further iterations due to the lag in the vorticity boundary conditions.

The ADEP method does not appear to work for the types of equations to be solved in this problem. No matter how small the time step irregularities soon build up in the field calculated.

The CDE method also does not appear to give satisfactory results. For example, as the temperature field is swept, alternative columns are updated.

The SE method would appear to be the most promising. The main disadvantage is the very small time step of 0·00002 which is required. Provided the time step is below the critical time

interval, very similar answers are obtained at a given time for different time intervals.

Davis and Thomas [13] used a procedure based on that used by Wilkes but incorporated an extra iteration step to update the boundary values of the vorticity. After computing the vorticity field using the boundary values from the previous time cycle, the vorticities at the boundaries were then recalculated from the new field and the interior values recalculated by ADIP.

For the results discussed here the boundary values of the vorticity along GH, HA, DE and EF were updated using the SE technique. Updated values along AB and CD were found according to Wilkes and then the remainder of the field computed by the ADIP method. By this means a time interval of approximately 20 times the time interval of the SE method can be used. Comparisons were made using the SE technique alone and using the combination of SE and ADIP. Excellent agreement was obtained.

Having determined the vorticity, the stream function was determined by systematic over-relaxation, using an over-relaxation factor of 1·60. With $\Delta X = 0{\cdot}0333$ and $\Delta Y = 0{\cdot}05$ the number of grid points is 741. Even though the starting field values where those from the previously converged solution convergence was slow. This was accelerated as follows. For each new vorticity field only the area bounded by $0 \leqslant \bar{X} \leqslant \frac{1}{2}$ and $0 \leqslant \bar{Y} \leqslant \frac{1}{4}$, i.e. within the channel proper was initially operated on by equation (16) to determine $\bar{\psi}$, with the assumption $\partial\bar{\psi}/\partial\bar{X} = 0$ at $\bar{X} = 0$. As each row was swept the value of $\bar{\psi}$ on the right hand boundary CD was determined so as to satisfy $\bar{U} = \partial\bar{\psi}/\partial\bar{Y} = 0$. After this reduced area had been swept the average value of $\bar{\psi}$ was determined. All values of $\bar{\psi}$ on this wall are replaced by this average before the next iteration is commenced as discussed in [14]. After the $\bar{\psi}$ field for this reduced area had converged the value of $\bar{\psi}$ and the value of $\bar{\psi}$ along DE and EF was set equal to the value on boundary CD. An initial $\bar{\psi}$ distribution was then calculated assuming a linear distribution from $\bar{\psi} = 0$ on the center line to the given value on EF. The $\partial\bar{\psi}/\partial\bar{X} = 0$ restriction at $\bar{X} = 0$ was then removed and the whole area was repeatedly swept until convergence was obtained.

Except for the method of updating the boundary values of the vorticity the solution technique is essentially that of [6].

HEAT TRANSFER

The Nusselt number is of practical importance as a measure of heat transfer from the plates to the fluid flowing up between the plates.

One definition of the Nusselt number depends on the rate of heat transfer from the plate to the fluid and has been extensively used as in [3–6].

The heat flux per unit width of the cavity (in the z-direction) leaving the right hand plate is

$$q = -\int_0^L k\left(\frac{\partial T}{\partial y}\right)_{y=+d} \mathrm{d}x \tag{23}$$

and in terms of a mean heat transfer coefficient by

$$q = -h_m L(T_w - T_0). \tag{24}$$

Defining the Nusselt number as

$$Nu_a = h_m 2d/k \tag{25}$$

and after normalizing the following is obtained

$$Nu_a = \frac{n}{m}\cdot\frac{1}{(Bb\bar{Y}^{b-1} + 1 - B)_{\bar{y}=\frac{1}{4}}} \int_0^{\frac{1}{2}}\left(\frac{\partial\bar{T}}{\partial\bar{Y}}\right)_{\bar{y}=\frac{1}{4}} [Aa\bar{X}^{a-1} + 1 - A]\,\mathrm{d}\bar{X}. \tag{26}$$

The Nusselt number as now defined decreases with time as $(\partial T/\partial\bar{y})$ decreases with time.

The heat added to the fluid between entry and exit is given by

$$H = \int_{-d}^{+d} \rho uc(T_{BC} - T_0)\,\mathrm{d}y. \tag{27}$$

An average surface conductance over the channel height can be defined by

$$a = H/2L(T_w - T_0). \tag{28}$$

Defining the Nusselt number by

$$Nu_b = ad/k \tag{29}$$

and normalizing using equations (3) the following is obtained

$$Nu_b = Pr\left(\frac{m}{4w}\right)\int_{-\frac{1}{2}}^{+\frac{1}{2}} \overline{U}\,\overline{T}_{BC}(Bb\overline{Y}^{b-1} + 1 - B)\,d\overline{Y}. \tag{30}$$

This form has been used in [1] and [2]. Starting from $T = 0$ at $t = 0$, the value of Nu_b as defined will increase from zero to a maximum value at steady state, being a measure of the quantity of heat added to the fluid.

CLOSED FORM SOLUTION

A closed form solution only exists for fully developed steady state flow where all derivatives in the x direction are zero.

The basic equations are

$$\nu\frac{\partial^2 u}{\partial y^2} + g\beta(T - T_0) = 0 \qquad \text{from equation (1)(31)}$$

$$\frac{\partial^2 T}{\partial y^2} = 0 \qquad \text{from equation (4)(32)}$$

For the given boundary conditions these equations yield $\overline{T} = 1{\cdot}0$ and

$$\overline{U} = Gr/8\,[1 - 4m^2\bar{y}^2]. \tag{33}$$

The heat transfer characteristics are given by

$$Nu_a = 0{\cdot}0; \qquad Nu_b = GrPr/48w. \tag{34}$$

RESULTS

Detailed results are presented for a Prandtl number of 0·733 and Grashof numbers of 100 and 10 000.

For Grashof number of 100, Fig. 3 illustrates the behavior of the system starting from rest with the temperature steady at ambient conditions and all velocities are zero. Temperatures, velocities, and the maximum value of the stream function increases to a steady state value. The Nusselt number Nu_a decreases whilst Nu_b increases to their steady values. However, of more

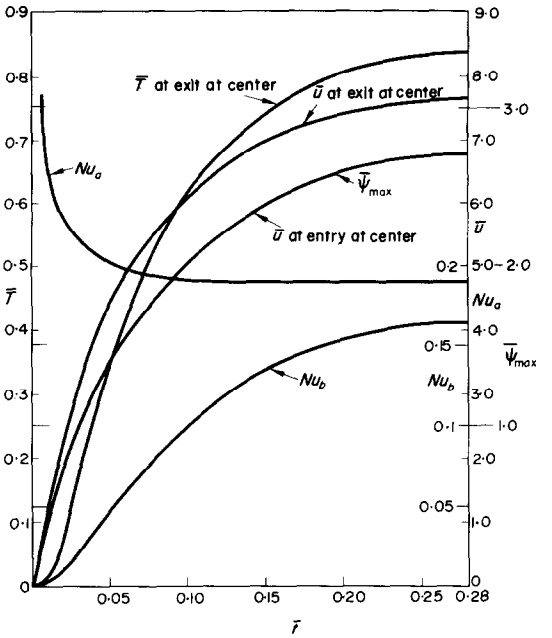

FIG. 3. Calculated values for Grashof number = 100·0.

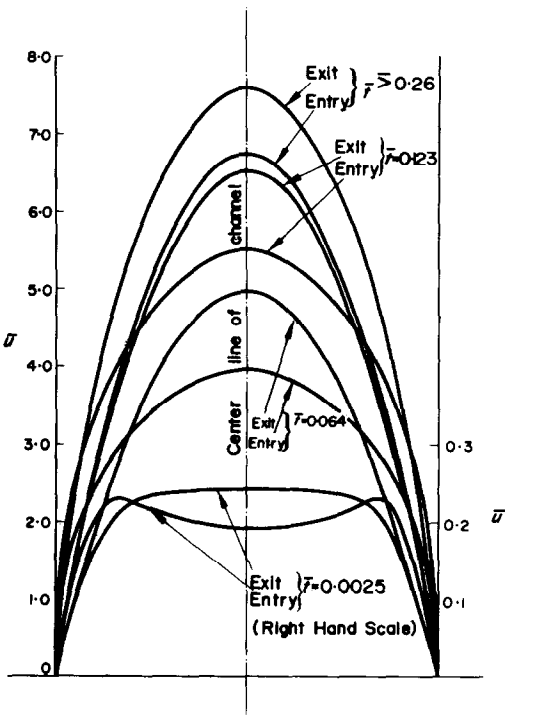

FIG. 4. Distribution of vertical velocity at top and bottom of channel, Gr = 100·0.

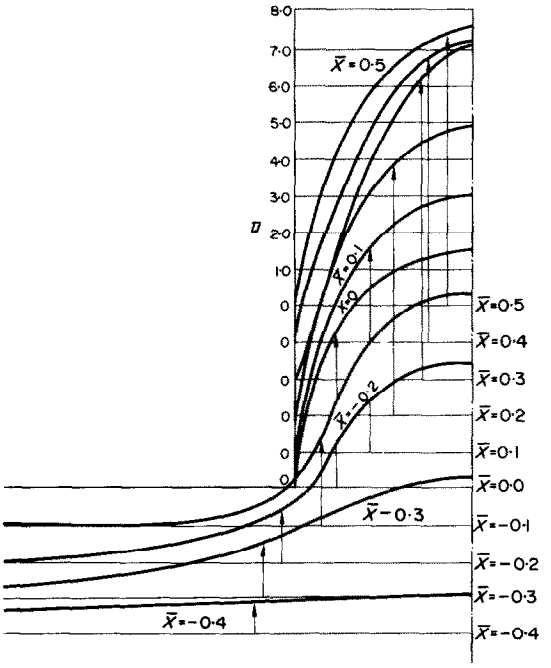

FIG. 5. Steady state velocity distributions—U Component—for Grashof number = 100·0.

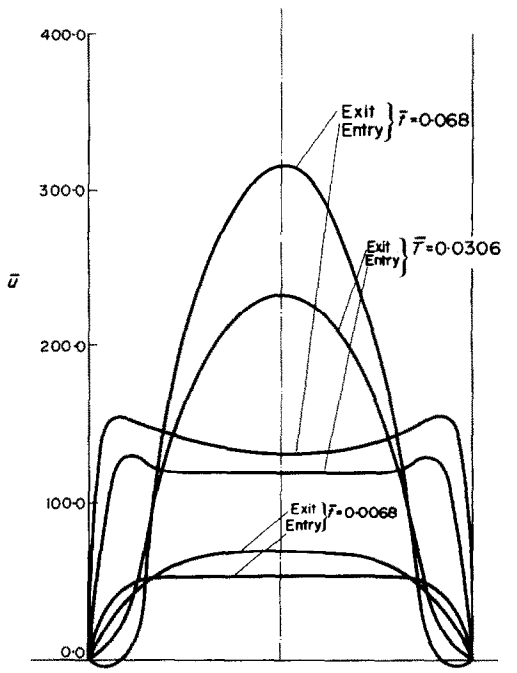

FIG. 7. Distribution of velocity at top and bottom of channel, Gr = 10 000·0.

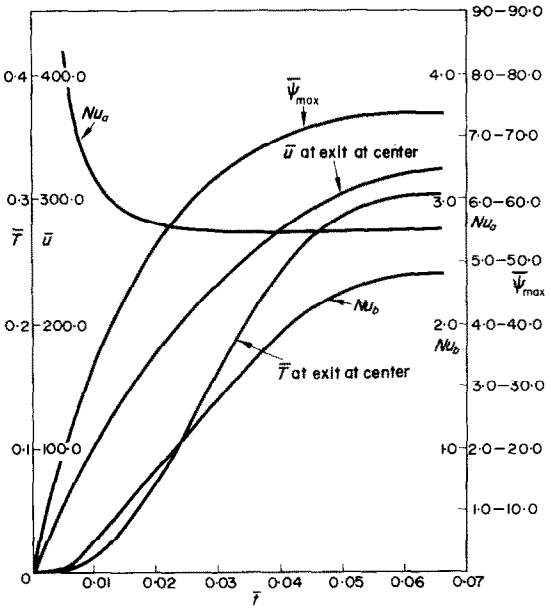

FIG. 6. Calculated values for Grashof number = 10 000·0.

interest is the velocity distribution. Figure 4 shows the velocity profiles at the top and bottom of the channel. At small times the inlet velocity distribution has a local minimum on the channel axis and a pair of symmetrically placed maxima on either side of it. A flat velocity profile exists at the exit. However, the velocity profiles soon take on a shape with a peak at the center line.

At steady state conditions the velocity distribution at different elevations of the channel and below the entrance are shown in Fig. 5. The required velocity profile begins to develop before entry to the channel.

Figure 6 illustrates the behavior of the system starting from rest but for a Grashof number of 10 000. Except for different numerical values the behavior pattern is similar to that for a Grashof number of 100. However, an examination of Fig. 7, which shows the velocity profile at different values of time, shows some marked differences from those developed when Gr = 100.

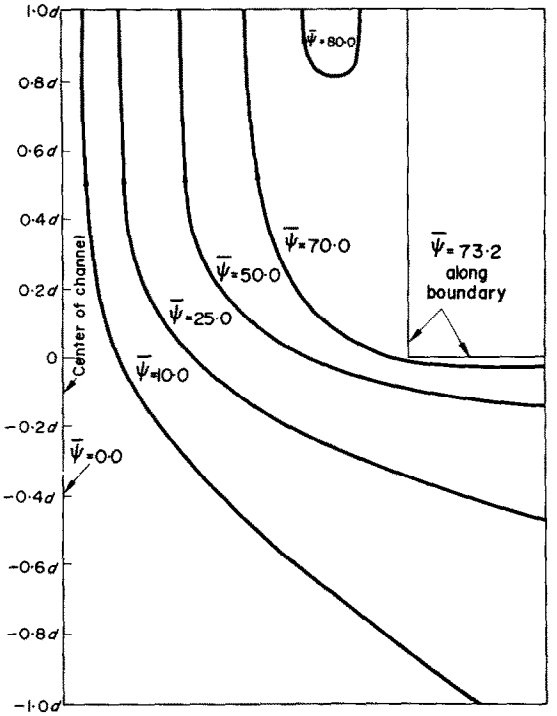

FIG. 8. Streamlines at entrance to channel, steady state conditions, $Gr = 10\,000{\cdot}0$.

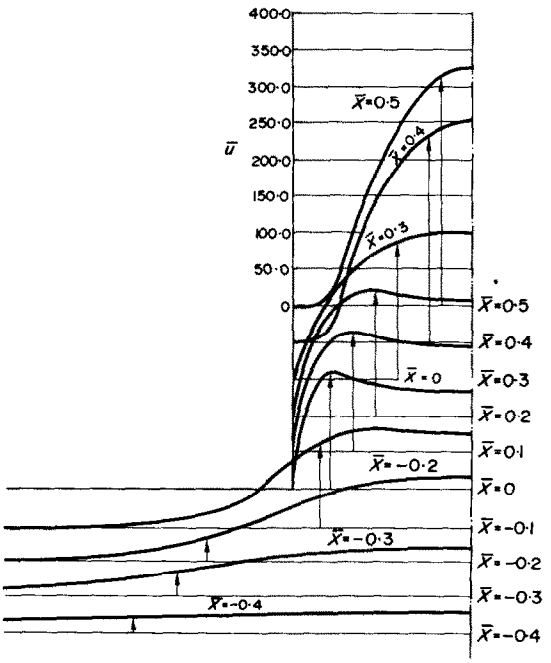

FIG. 9. Steady state velocity distributions—U component—for Grashof number = 10 000·0.

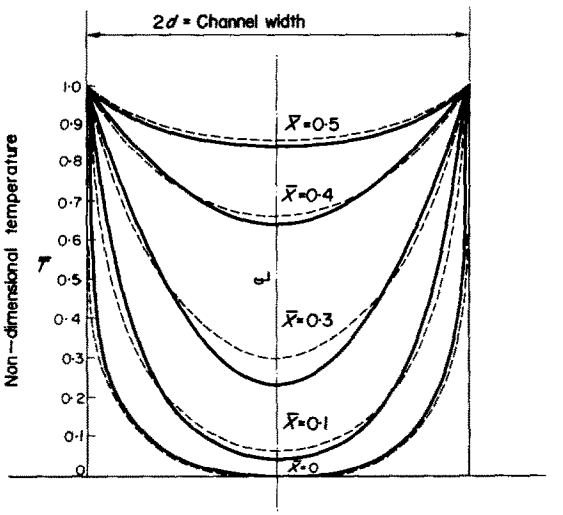

FIG. 10. Steady state temperature distribution; $Gr = 0{\cdot}0$ (dotted line), $Gr = 100{\cdot}0$ (full line).

At the entry section the profile retains for all time a local minimum on the channel axis and a pair of symmetrically placed maxima on either side of it. At exit the velocity distribution has a maximum on the center line, looking much like a parabolic distribution. At advanced times some reversed flow takes place near the channel sides. A plot of the streamlines for steady state

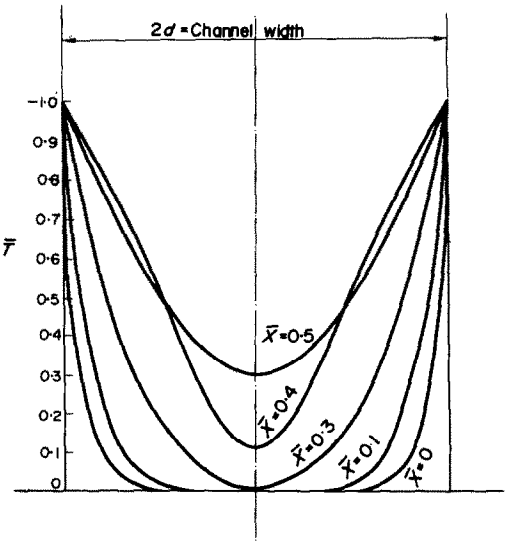

FIG. 11. Steady state temperature distribution; $Gr = 10\,000{\cdot}0$.

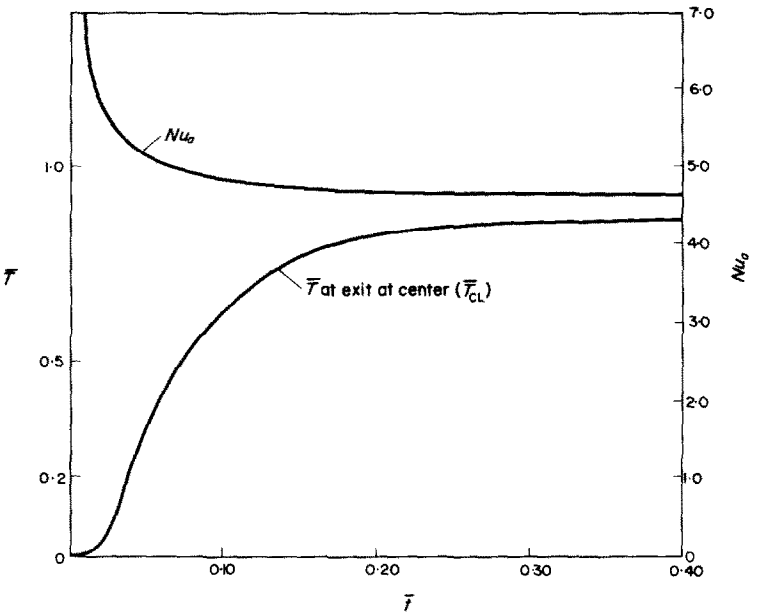

FIG. 12. Nusselt number Nu_a and exit center line temperature; $Gr = 0{\cdot}0$.

conditions ($Gr = 10\,000$) is shown in Fig. 8. It would appear that the buoyancy forces produced by the larger temperature difference associated with a Grashof number is so strong that the fluid is accelerated up the channel axis. There is also a relatively large v component of velocity at entrance. In order to maintain continuity, air is drawn in from above.

At steady state conditions the velocity distribution at different elevations of the channel and at various levels below the channel are shown in Fig. 9. The local maxima begins to form below the entrance region and is maintained for some distance up the channel before reversed flow takes place.

Figures 10 and 11 show steady state temperature distributions for Grashof numbers of 0, 100 and 10000 respectively. In all cases the minimum temperatures are on the center line. The maximum temperature on the center line at exit decreases as the Grashof number increases; these temperatures are 0·870, 0·840 and 0·305 for Grashof numbers equal to 0, 100 and 10000 respectively. In the limiting case of a very large Grashof number the problem is that of free convection from a heated vertical plate, when the two walls of the channel can be considered to be two vertical plates spaced at a considerable distance apart. A boundary layer is formed on each plate with the temperature on the center line between them remaining at the ambient temperature ($\bar{T} = 0{\cdot}0$). However, under these extreme conditions the reversed flow already discussed will not take place. Figure 12 shows the time history of Nu_a and $\bar{T}_{cl}$ when the Grashof number is zero. It is interesting to note that by comparing Figs. 3, 6 and 12 the time taken to reach steady state conditions increases as the Grashof number decreases. The value of Nu_a increases with increasing Grashof number. The buoyancy forces increase with increasing Grashof number, and the increased velocity of the fluid means that the time for the fluid to heat up is less. Hence the resulting exit temperature is less as the Grashof number increases.

Figure 11 illustrates an interesting effect at high Grashof numbers—the exit temperature distribution is not a maximum for the whole

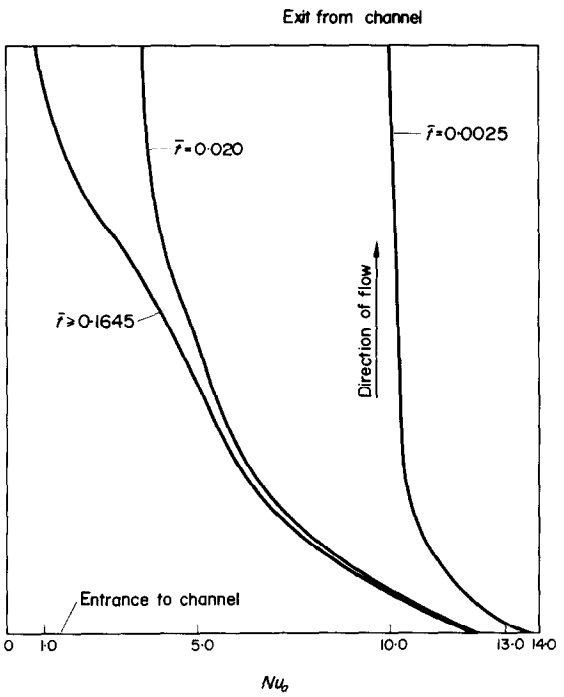

FIG. 13. Variation of Nu_a as fluid flows up channel, Grashof number = 100·0.

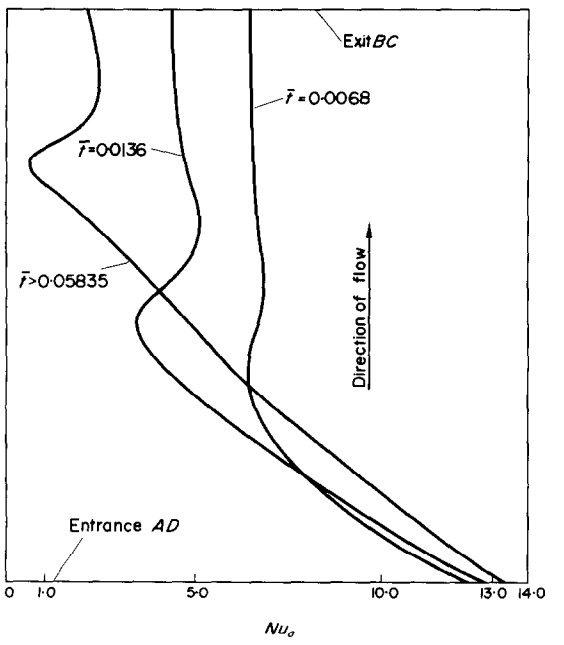

FIG. 14. Variation of Nu_a as fluid flows up channel, Grashof number = 10000·0.

channel width. Due to the small downward circulation of air near the plate as already described the fluid is actually cooler at the top; this can be seen by comparing temperatures at $\bar{X} = 0{\cdot}4$ and $\bar{X} = 0{\cdot}5$. The steady state temperature distribution shown in Fig. 11 shows the fluid is heated continuously as it flows upwards, and as the velocity is much smaller the resultant temperature is much greater.

The value of Nu_a depends on the temperature gradient at the wall, and its variation with channel height position is shown in Figs. 13 and 14. For a Grashof number of 100, the local value of Nu_a decreases as the fluid flows up the channel. being a minimum at the top. For a Grashof number of 10000 the effect of the maximum temperature gradient not occurring at exit is clearly demonstrated by a local reduction in the Nusselt number. This local reduction is more marked and moves up the channel as the motion proceeds in time, as shown in Fig. 14.

A comparison is made between these results and the work reported in [1]. For a value of $Gr = 10000$ and $Pr = 0{\cdot}733$, Fig. 8 of [1] gives a value of Nu_b of about 1·9 compared with 2·38 calculated here. The experimental work used square plates, and hence side leakage would take place and would reduce the heat transfer and hence the Nusselt number. The deviation between experiment and computed results increases as the Grashof number decreases where the close plate separation results in increased side leakage. The temperature attained by the fluid leaking at the side will be less than that attained had the fluid travelled the full length of the passage, and thus the experimental Nusselt number is decreased.

CONCLUSIONS

No attempt has been made to study the full range of Grashof numbers. For a Grashof number of 10000 with a time interval of 0·00015 the time taken on an IBM 360/65 was 35 min to run to steady state. For a Grashof number of 100 the stable time limit was 0·0005. However, it took much longer (in real time) for

steady state conditions to be reached and the time taken on the computer to run to steady state was about 40 min. The mesh size in the y-direction was 0·05 (41 mesh points) and in the x-direction the mesh size was 0·0333 (46 mesh points). No attempt has been made to solve for a large number of cases because of the computor time required.

The results showed that for small Grashof numbers a "parabolic" type velocity distribution existed at entry; for high Grashof numbers a velocity distribution with a minimum at the center existed at steady state. Also at higher values of the Grashof number the buoyancy forces are so strong that fluid is drawn down from above at the sides. The existence of a velocity profile with a local minimum on the channel axis and a pair of symmetrically placed maxima on either side of it has been discussed by several authors when dealing with entrance flow characteristics and assuming an entrance velocity distribution which is rectangular. However, this appears to be the case when the entrance velocity distribution is formed naturally.

Table 2. Typical computed values

Gr	0	100·0	10000·0
Nu_b	0	0·164	2·38
Nu_a	4·64	4·75	5·50
$\bar{\psi}_{max}$	0	2·73	73·5
$\bar{U}_{max}$	0	7·65	325·0
$\bar{T}_{cl}$	0·860	0·835	0·305
Time to Steady State	0·375	0·260	0·065

Table 2 gives some main details of the computational results. As the Grashof number increases, the Nusselt number, the quantity of flow and the maximum velocity at exit increases. However, with increasing Grashof number the time taken to reach steady state decreases as well as the exit center line temperature. As the Grashof number increases the large induced vertical velocity causes an increase in the heat carried away by convection; at the same time the heat conduction perpendicular to the main flow is much smaller and hence, the fluid does not remain long enough in the channel to be heated up to a temperature approaching the wall temperature.

Table 3 shows certain computed values derived from the closed form solution. These only give a bound for the values shown in Table 2. The two sets of answers approach each other as the Grashof number decreases. However, no attempt can be made to compare Tables 2 and 3 as the latter is based on fully developed flow throughout the channel.

Table 3. Typical values for fully developed flow. $\partial/\partial x = 0$

Gr	0	100·0	10000·0
Nu_b	0	0·30	30·40
Nu_a	0	0	0·0
$\bar{\psi}_{max}$	0	4·17	417·0
$\bar{U}_{max}$	0	12·50	1250·0
$\bar{T}_{cl}$	1·0	1·0	1·0

At relatively high Grashof numbers the separation of the boundary layer which takes place at some distance from the leading edge at the entrance to the channel appears to account for the reversed flow already discussed. This phenomena needs more investigation and further work is being pursued on a single plate under conditions where the fluid has to flow round a corner as at the channel entrance rather than the case of a thin vertical plate with symmetrical flow conditions.

ACKNOWLEDGEMENT

Acknowledgement with thanks is made to Wen Ho Lee who carried out much of the program development on the I.B.M. 360/65 computer of Texas A & M University.

REFERENCES

1. J. R. Bodoia and J. F. Osterle, The development of free convection between heated parallel plates, *J. Heat Transfer* **84**, 40–44 (1962).
2. J. R. Dyer and J. H. Fowler, The development of natural convection in a partially-heated vertical channel formed by two parallel surfaces, *Trans. Instn Engrs Aust.* **MC1**, 12–16 (1966).
3. G. de Vahl Davis, Laminar natural convection in an enclosed rectangular cavity, *Int. J. Heat Mass Transfer* **11**, 1675–1693 (1968).
4. G. de Vahl Davis and C. F. Kettleborough, Natural

convection in an enclosed rectangular cavity, *Trans. Instn Engrs Aust.* **MC1**, 43–49 (1965).
5. F. LANDIS and H. YANOWITZ, Transient natural convection in a narrow vertical cell, *Proc.* Third Int. Heat Transfer Conf. A.I.Ch.E., New York (1966).
6. J. O. WILKES and S. W. CHURCHILL, The finite difference computation of natural convection in a rectangular enclosure, *A.I.Ch.E. Jl* **12**, 161–166 (1966).
7. H. Z. BARAKAT and J. A. CLARK, On the solution of the diffusion equation by numerical methods, *J. Heat Transfer* **88**, 421–427 (1966).
8. B. K. LARKIN, Some stable explicit difference approximations to the diffusion equation, *Maths Comput.* **18**, 196–202 (1964).
9. D. QUON, P. M. DRANCHUK, S. R. ALLADA and P. K. LEUNG, Application of the alternating direction explicit procedure to two-dimensional natural gas reservoirs, *Soc. Petrol. Engrs Jl* **6**, 137–142 (1966).
10. K. H. COATS and M. H. TERHUME, Comparison of alternating direction explicit and implicit procedures in two dimensional flow calculations, *Soc. Petrol. Engrs Jl* **6**, 350–362 (1966).
11. R. K. MACGREGOR and A. F. EMERY, Free convection through vertical plane layers—moderate and high Prandtl number fluids, *J. Heat Transfer* **91**, 391–403 (1969).
12. J. E. FROMM, A method for computing nonsteady, incompressible, viscous fluid flows, Low Alamos Scientific Laboratory, Report No. LA-2910 (1963).
13. G. DE VAHL DAVIS and R. W. THOMAS, Natural convection between concentric vertical cylinders, *Physics Fluids*, Suppl II, 198–207 (1969).
14. P. J. TAYLOR, The stability of boundary conditions in the numerical solution of the time-dependent Navier–Stokes equations, Aeronatutical Research Council A.R.C. 30 406 (August 1968).

CONVECTION NATURELLE LAMINAIRE TRANSITOIRE AVEC EFFET D'ENTREE ENTRE DES PLAQUES VERTICALES CHAUFFEES

Résumé—On décrit une étude numérique du mouvement bidimensionnel laminaire transitoire d'un fluide entre deux plaques chauffées verticales, le mouvement étant généré par un gradient de température perpendiculaire à la direction de la force de volume. Le développement de l'écoulement dans la région d'entrée est particulièrement intéressant. Les résultats montrent que partant des conditions initiales de repos, la vitesse croît à chaque plaque en formant deux couches limites qui se fondent progressivement en une seule entre les plaques.

Pour un temps cours le profil de vitesse à l'entrée du canal a un minimum local sur l'axe et une paire de maximums symétrique par rapport à cet axe. Néanmoins pour les faibles nombres de Grashof ce profil à l'entrée se modifie en un autre possédant un maximum au centre pour des temps plus longs. Pour les nombres de Grashof plus grands le profil à l'entrée qui a encore une paire de maximums devient une distribution de type normal lorsque le fluide progresse dans le canal. Dans tous les cas les deux frontières verticales sont à la même température constante. Les caractéristiques du transfert thermique sont apportées au nombre de Nusselt.

Des distributions typiques de température et de vitesse sont données pour des nombre de Grashof compris entre 100 et 10.000 le nombre de Prandtl étant toujours égal à 0,73. Différentes techniques numériques sont discutées pour résoudre les équations de l'énergie et de la vorticité.

INSTATIONÄRE LAMINARE FREIE KONVEKTION ZWISCHEN BEHEIZTEN SENKRECHTEN PLATTEN UNTER BERÜCKSICHTIGUNG VON EINLAUFEFFEKTEN

Zusammenfassung—Es wird eine numerische Untersuchung beschrieben über die instationäre laminare, zweidimensionale Strömung eines Fluids zwischen zwei beheizten senkrechten Platten, wobei die Strömung durch den Temperaturgradienten senkrecht zur Richtung der Schwerkraft hervorgerufen wird. Von besonderem Interesse ist die Ausbildung der Strömung am Einlauf. Die Ergebnisse zeigen, dass, ausgehend vom Ruhezustand. sich an jeder Platte eine Grenzschicht ausbildet. Sie wachsen zusammen. wenn sich das Fluid zwischen den Platten nach oben bewegt.

Für kleine Zeiten hat das Geschwindigkeitsprofil am Eintritt in den Kanal ein Minimum in der Kanalachse und ein Paar symmetrisch angeordneter Maxima links und rechts davon. Für kleine Grashofzahlen jedoch geht dieses Einlaufprofil mit fortschreitender Zeit in ein Profil mit einem Maximum in der Mittelachse über. Für grössere Grashofzahlen hat das Einlaufprofil immer zwei Maxima und geht mit aufwärtsströmendem Fluid in ein "normalverteiltes" Profil über. In jedem Fall hatten die beiden vertikalen Grenzen die gleiche konstante Temperatur. Der Wärmeübergang wurde als Funktion der Nusseltzahl berechnet.

Typische Temperatur- und Geschwindigkeitsverteilungen werden für Grashofzahlen von 100 und 10000 angegeben; in beiden Fällen ist die Prandtlzahl 0,73. Verschiedene numerische Methoden zur Lösung der Energie- und der Wirbelgleichungen werden diskutiert.

НЕСТАЦИОНАРНАЯ ЛАМИНАРНАЯ СВОБОДНАЯ КОНВЕКЦИЯ МЕЖДУ НАГРЕТЫМИ ВЕРТИКАЛЬНЫМИ ПЛАСТИНАМИ, ВКЛЮЧАЯ ЭФФЕКТЫ НА ВХОДЕ

Аннотация—Описывается численное исследование нестационарного ламинарного двумерного движения жидкости между двумя нагретыми вертикальными пластинами, причем движение генерируется градиентом температуры, перпендикулярным направлению силы тяжести. Особый интерес представляет развитие потока во входной области. Результаты показывают, что, начиная с состояния покоя, скорость нарастает на каждой пластине, образуя два пограничных слоя, которые сливаются в один по мере перемещения жидкости вдоль пластин.

Для небольшого значения времени профиль скорости на входе в канал имеет локальный минимум на оси канала и пару симметрично расположенных максимумов с каждой стороны от неё. Однако для небольших значений чисел Грасгофа этот профиль на входе преобразуется в профиль с максимумом на центральной линии для более высоких значений времени. Для больших значений чисел Грасгофа профиль на входе всегда характеризуется парой максимумов, которые развиваются в «распределение обычного типа» по мере того как жидкость движется вверх по каналу. Во всех случаях обе вертикальные пластины находятся при постоянной температуре. Характеристики переноса тепла выражаются через число Нуссельта.

Типичные распределения температуры и скорости проводятся для чисел Грасгофа, равных 100 и 10 000. Для обоих случаев число Прандтля равнялось 0,73. Обсуждаются различные численные методы решения уравнений энергии и завихренности.